Alkanethiol-Passivated Ge Nanowires as High-Performance Anode Materials for Lithium-Ion Batteries: The Role of Chemical Surface Functionalization

Fang-Wei Yuan, Hong-Jie Yang, and Hsing-Yu Tuan*

Department of Chemical Engineering, National Tsing Hua University, 101, Section 2, Kuang-Fu Road, Hsinchu, Taiwan 30013, ROC

ABSTRACT We demonstrate that dodecanethiol monolayer passivation can significantly enhance the anode performance of germanium (Ge) nanowires in lithium-ion batteries. The dodecanethiol-passivated Ge nanowires exhibit an excellent electrochemical performance with a reversible specific capacity of 1130 mAh/g at 0.1 C rate after 100 cycles. The functionalized Ge nanowires show high-rate capability having charge and discharge capacities of ~555 mAh/g at high rates of 11 C. The functionalized Ge nanowires also performed well at 55 °C, showing their thermal stability at high working temperatures. Moreover, full cells using a $LiFePO_4$ cathode were assembled and the electrodes still have stable capacity retention. An aluminum pouch type lithium cell was also assembled to provide larger current (~30 mA) for uses on light-emitting-diodes (LEDs) and audio devices. Investigation of the role of organic monolayer coating showed that the wires formed a robust nanowire/PVDF network through strong C—F bonding so as to maintain structure integrity during the lithiation/delithiation process. Organic monolayer-coated Ge nanowires represent promising Ge—C anodes with controllable low carbon content (*ca.* 2—3 wt %) for high capacity, high-rate lithium-ion batteries and are readily compatible with the commercial slurry-coating process for cell fabrication.

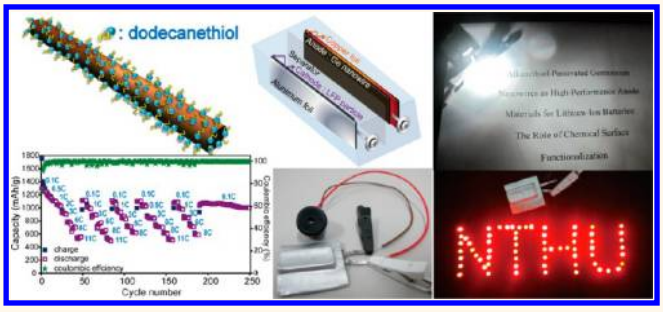

KEYWORDS: germanium · nanowires · dodecanethiol · surface passivation · lithium-ion battery

Rechargeable lithium-ion batteries have been widely used in portable electronic devices such as cell phones, laptop computers, and digital cameras, and have been considered as an electrochemical energy storage system for powering hybrid electric vehicles (HEV) and zero-emission vehicles (ZEV).[1,2] To satisfy the increasing demand, it is necessary to develop lithium-ion batteries having a higher energy density and a higher power density.[3] The graphite anode has been commonly used due to its stable rate capability and long cycle life; however, its relatively low capacity (372 mAh/g) limits the increase of energy storage. To increase the total battery capacity over 20%, one effective approach is to use graphite alternatives with high lithium capacity as anode materials.[4,5]

Germanium (Ge) has emerged as a promising graphite alternative due to its high theoretical gravimetric capacity of 1384 mAh/g at room temperature, only second to silicon (3579 mAh/g), among all Li-alloying materials.[2,6—13] The diffusivity of lithium in Ge is ~400 times greater than that of lithium in Si at room temperature, thus having high-rate capability. Ge's intrinsic electronic conductivity is 10^4 times higher than Si, giving much faster electron transport.[14] However, the practical usage of Ge as an anode material is hindered by dramatic volume changes (~300%) caused by insertion/extraction of lithium ions, which results in crack and pulverization, and loss of electrode contact. In early studies, micrometer-sized Ge particles exhibited poor electrochemical performance due to a rapid capacity fading. Recently, Ge nanomaterials such as nanoparticles,[15—21] nanowires,[22—34] and nanotubes[35] have been synthesized. These nanostructures effectively accommodate the volume changes, tolerate relaxed mechanical strain, and alleviate

* Address correspondence to hytuan@che.nthu.edu.tw.

Received for review August 4, 2012 and accepted October 8, 2012.

Published online 10.1021/nn303519g

pulverization.[36−38] Particularly, nanowires not only relax volume strain, but also provide channels for efficient electron transport along through the length.[14,37] For instance, high reversible capacities of Si and Ge nanowires were attainable by direct growth of wires on current collector substrates using the vapor−liquid−solid (VLS) method.[37,38] On the other hand, there appears a need to incorporate nanomaterials into a slurry-coating process which is more compatible with commercial realization. Slurry comprising a mixture of active material, conducting addictive, and binder was coated onto a current collector to form a composite electrode. The slurry-coating process allows a large amount of electrode materials assembled onto the current collector. Direct incorporation of Si and Ge nanowires into the slurry-coating process showed improved electrochemical performance relative to microparticles; however, the anode performance decayed rapidly within a few tens of cycles. One effective approach to improve Si and Ge nanowire's cycling performance is to use carbon-based composites because carbon acts as an electron conductor to allow Li ion transport between the electrode and current collector and serves as a soft matrix to reduce structure distortion.[39−48] For example, electrodes composed of a mixture of carbon-coated Si nanowires and carbon nanotubes exhibited improved lithium capacity relative to raw nanowires.[39] Ge nanowires sheathed with amorphous carbon showed a stable reversible charge capacity.[40] However, reactions to form carbon-based Ge composite are mostly associated with complicated, high-temperature and multiple-step procedures. Moreover, the carbon content is hard to control, accounts for a large portion in the composites, and suppresses the overall electrode capacity.

Chemical surface functionalization is important to Si and Ge nanowires since their surface-related properties are more pronounced relative to their bulk surfaces.[49−61] Organic monolayer passivation of nanowires gave rise to many advantageous properties such as better oxidation resistance, improved electrical characteristics, and stable solvent dispersibility. Functionalized Ge nanowires are more implementable into solvent-based processing for a variety of applications.[49,53,59] Alkene- and alkanethiol-passivated Ge nanowires showed surface stability up to 1 month under ambient conditions and exhibited excellent corrosion resistance against harsh environments.[52,58] In addition, organic monolayer functionalization can also efficiently tune surface properties to interface with other materials. For instance, dodecene-functionalized Ge nanowires were well-dispersed in Kraton polymer for composite fabrication.[53] It is also important to note that many organic ligand passivation reactions, such as thiolation reactions, are facile, mild, and scalable to be applied to material functionalization.

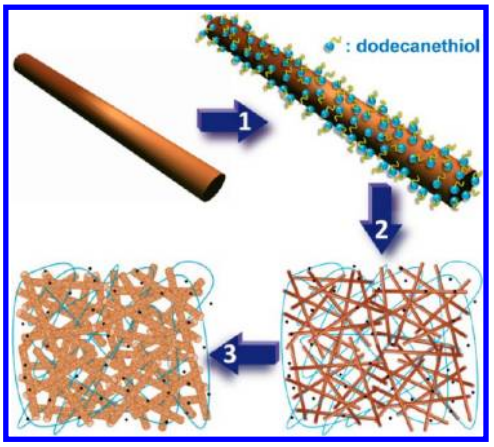

Figure 1. Scheme of dodecanethiol-passivated Ge nanowires as anode materials for lithium-ion batteries. (1) Ge nanowires were functionalized with dodecanethiol monolayers at 80 °C under Ar atmosphere. (2) Ge nanowire anodes were prepared *via* a conventional slurry-coating process. The small black particles indicate carbon black and blue lines indicate PVDF chains. (3) Ge nanowire/PVDF network structure formed after Li charge/discharge cycles.

Here we show that dodecanethiol monolayer passivation can significantly enhance the anode performance of Ge nanowires in lithium-ion batteries. As illustrated in Figure 1, thiolation of Ge nanowires was carried out in the presence of dodecanethiol at 80 °C under argon atmosphere. Dodecanethiol-passivated Ge nanowires were then proceeded through a slurry-coating process for lithium-ion anode fabrication. The functionalized nanowires afford superior electrochemical performances with a reversible capacity of 1130 mAh/g when cycled 100 times at a cycle rate of 0.1 C (a rate of 1 C corresponds to full charge or discharge in one hour). The capability to serve as high performance anodes is demonstrated through five different charge and discharge rates, each for 50 cycles, and five high-rate cycling periods in 250 cycles. The nanowires deliver charge and discharge capacities of ∼555 mAh/g at rates of 11 C, nearly 2 times higher than graphite at such high cycling rates. The thermal stability of the Ge nanowire electrode operated at 55 °C is investigated. The electrochemical performance of the dodecanethiol-passivated Ge nanowire ranks among the best of nanowire-based anodes reported to date. The role of organic monolayers related to nanowire structure integrity was investigated. Alkanethiol-passivated Ge nanowires represent novel low-carbon-loaded Ge−C anode materials made without the need of complex reactions and can be potentially used for high-performance lithium-ion battery applications. Importantly, this work highlights the organic ligand's positive effect on Ge's lithium-ion storage performance, which may be applied to more electrode systems. Finally, full cells were assembled using dodecanethiol-passivated Ge nanowires as an anode and $LiFePO_4$ particles as a cathode for uses on different electronic devices.

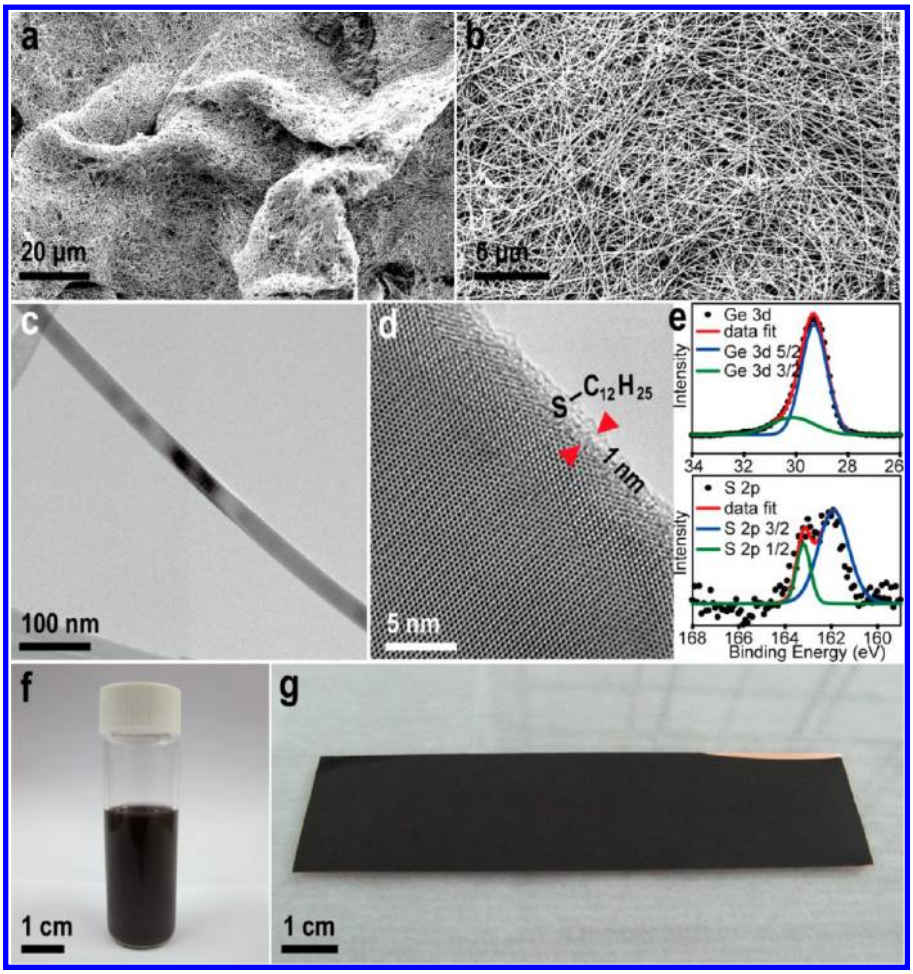

Figure 2. (a,b) SEM images of Ge nanowires passivated with dodecanethiol monolayers. (c) TEM image of an individual Ge nanowire. (d) HRTEM image of a dodecanethiol-passivated Ge nanowire. Notice the absence of the surface oxide layer but externally coated with a 1 nm organic layer. (e) Ge 3d and S 2p XPS of functionalized Ge nanowires shows the absence of oxide characteristic peaks. (f) Photograph of Ge nanowires well-dispersed in NMP without aggregation. (g) Photograph of a Cu foil coated with an anode film of Ge nanowires.

RESULTS AND DISCUSSION

Preparation of Dodecanethiol-Passivated Ge Nanowires. Ge nanowires were synthesized using the gold-seeded supercritical fluid−liquid−solid (SFLS) method.[62,63] As-prepared wires were coated with an oxide layer of approximately 3 nm due to oxidation under ambient surrounding (Supporting Information, Figure S1). Chemical surface passivation of Ge nanowires began by the etching with diluted HF to remove the oxide layer followed by functionalization with dodecanethiol (see Methods section for detail). Figure 2 panels a and b show SEM images of great surface smoothness of dodecanethiol-passivated Ge nanowires. The wires have an average diameter of approximately 45 nm and a length longer than 100 μm. The HRTEM image of a Ge nanowire shows a single crystalline nature, externally coated with an amorphous layer shell with a thickness around 1 nm, that agrees with the length of a C_{12}-thiol group (Figure 2c,d).[50] The XPS peak of Ge 3d spectrum of dodecanethiol-passivated Ge nanowires was identified for no noticeable Ge oxide signal (Figure 2e). On the basis of CHNS analysis, the carbon content of dodecanethiol-passivated Ge nanowires is around 2.7−2.9 wt % (Supporting Information, Table S1). The Ge nanowire mat was homogeneously mixed with poly(vinylidene fluoride) (PVDF) binder and carbon black in NMP (Figure 2f). After the removal of NMP under mild heating overnight, the composite electrode was uniformly coated on a copper foil which served as a current collector. Figures 2g shows the photograph of the prepared Ge anode.

Electrochemical Performance of Dodecanethiol-Passivated Ge Nanowire Anodes in Lithium-Ion Batteries. Figure 3a shows galvanostatic cycling results of dodecanethiol-passivated Ge nanowires, unpassivated Ge nanowires, and commercial Ge powders at a rate of 0.1 C rate between 1.5 and 0.01 V in coin-type half cells. The capacity of Ge powders quickly dropped to ~280 mAh/g after only several cycles. The rapid decrease of capacity indicated that microsized Ge particles pulverize due to large volume change during the Li alloying/dealloying process and results in electrically disconnected small

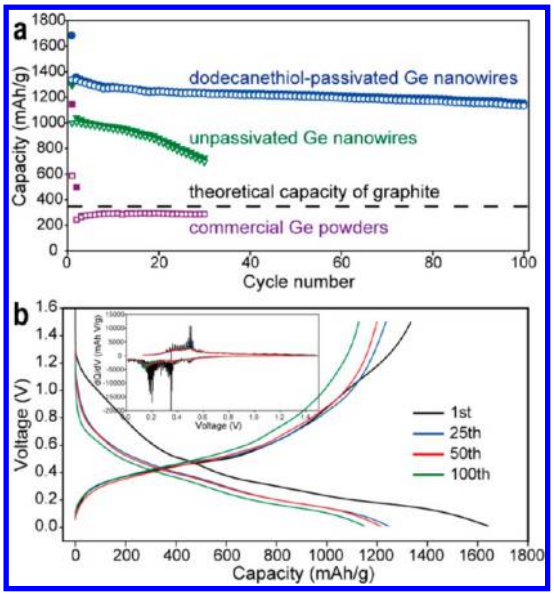

Figure 3. (a) Charge/discharge cycle performance of dodecanethiol-passivated Ge nanowires, unpassivated Ge nanowires, and commercial Ge powders at a rate of 0.1 C between 0.01 and 1.5 V: (filled symbol) charge; (open symbol) discharge. (b) Voltage profiles of the functionalized Ge nanowires at the 0.1 C rate. Inset shows differential capacity plots of the 1st, 25th, 50th, and 100th cycle, respectively.

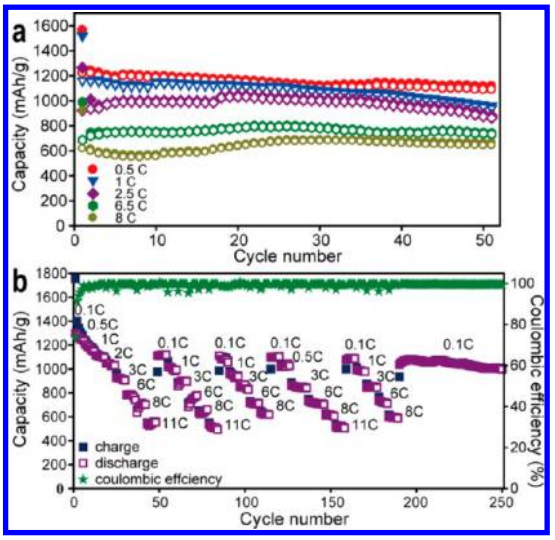

Figure 4. (a) Charge/discharge cycle performance of dodecanethiol-passivated Ge nanowires at rate of 0.5 to 8 C between 0.01 and 1.5 V: (filled symbol) charge; (open symbol) discharge. (b) Charge/discharge profiles of dodecanethiol-passivated Ge nanowires cycled at various rates.

fragments. The first charge capacity of the unfunctionalized Ge nanowire anode was 1291 mAh/g and the first discharge capacity was 998 mAh/g, corresponding to a Coulombic efficiency of 77.3%. The observed irreversible capacity in the first cycle is mostly likely due to the formation of solid electrolyte interface (SEI) layer which increased internal resistance and caused impedance of Li ion transport. The capacity was around 1000 mAh/g after the second cycle, giving a relatively higher capacity than commercial Ge powders. However, the capacity rapidly faded at the consecutive cycles. As shown in the TEM images of electrode after cycle tests (Supporting Information, Figure S2), Ge nanowires were disintegrated into small, isolated fragments. It may be possibly that Ge nanowires became soft and fragile after repeated cycles. The possibility of aggregation of Ge nanowires that induced crack initiate could not be ruled out. After battery tests, the nanowire electrode was unstable and gradually pulverized and peeled off, making capacity fade rapidly.

Dodecanethiol-passivated Ge nanowires had a high reversible specific capacity. At a 0.1 C rate, the first charge and discharge capacities were respectively, 1680 and 1332 mAh/g, which corresponds to a Coulombic efficiency of 79.3%. The improved Coulombic efficiency might be attributed to the decreased formation of the SEI layer. The first cycle of received discharge capacity of 1332 mAh/g is almost identical to the theoretical capacity of Ge nanowires. The better capacity performance might be resulted from efficient Li transport through the Ge wire electrode. At each of the subsequent 99 cycles at 0.1 C, that is, second to 100th cycle, the Coulombic efficiency was over 99%. The capacity retention of the Ge nanowires was 1130 mAh/g after 100 cycles. As shown in the voltage profile, the voltage decreased steeply from the open circuit voltage to 0.6 V where a plateau region set in and continued until a specific capacity of 1680 mAh/g was reached for the first charge. In the first discharge profile, a plateau at 0.3 V could be obviously observed (Figure 3b) The voltage plateaus appeared at the same region at the subsequent cycles, consistent with the behavior of Ge lithium ion anode in previous reports.[38,40,43]

We also examined the anode performance of dodecanethiol-passivated Ge nanowires at high charge/discharge rates. During cycling tests, charge and discharge rates were kept the same for 50 cycles to obtain valuable information of high-rate performance of nanowire electrode for most potential applications. Figure 4a shows the capacity at cycling rates of 0.5, 1, 2.5, 6.5, and 8 C in the range of 0.01 V and 1.5 V *versus* Li/Li^+. The recorded discharge capacities were 1090 mAh/g (0.5 C), 940 mAh/g (1 C), 865 mAh/g (2.5 C), 733 mAh/g (6.5 C), and 644 mAh/g (8 C) when cycled 50 times. Although the irreversibility of capacity was still observed in the first charge/discharge cycle, the Coulombic efficiency remained over 98% at each cycle during the second cycle to 50th cycle, suggesting excellent cycling stability at high rates. The charge and discharge capacities of ~644 mAh/g at 8 C rate is almost two times higher than the theoretical capacity of graphite. To examine capacity stability at different rates in a reasonable long period, the anode was tested at different current rates up to 250 cycles (Figure 4b). The Ge nanowires still delivered charge

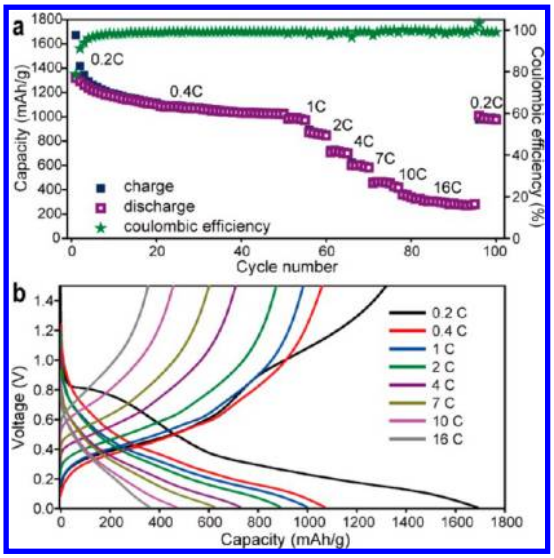

Figure 5. (a) Cycle performance and (b) galvanostatic charge/discharge profiles of dodecanethiol-passivated Ge nanowires cycled at various rates from 0.2 to 16 C. The experiment was carried out at 55 °C in a CR2032 coin-type half-cell.

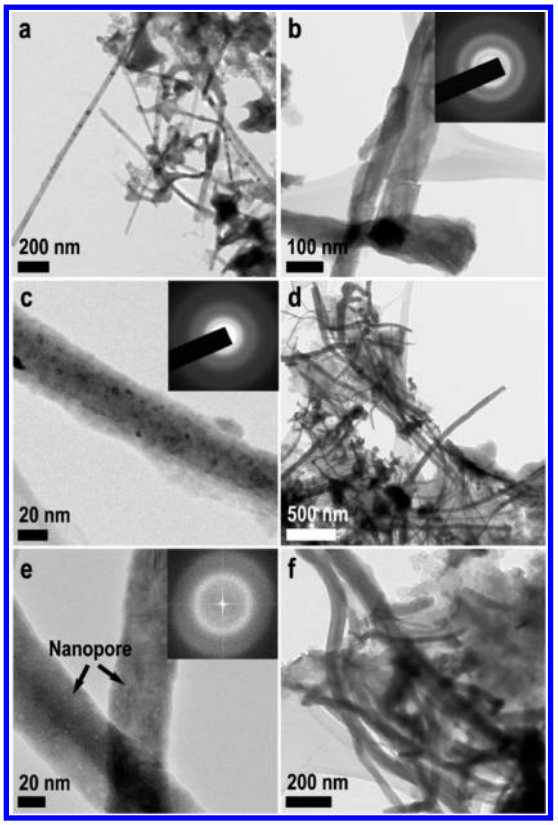

Figure 6. Microstructure evolution of dodecanethiol-passivated Ge nanowires: (a) before and (b–f) after electrochemical cycling in a lithium-ion cell. During the first cycle charged to 0.01 V, a single crystalline Ge nanowire partly converted to an amorphous Li_xGe nanowire as shown in the SAED (inset) (b). While discharged to 1.5 V, the nanopore formed (c), a nanowire/PVDF sponge network was observed, and the nanowire becomes mostly amorphous Ge (inset) (d). After the second lithiation/delithiation process, nanopores emerged more clearly inside the nanowires and the network structure was still observed (e,f).

and discharge capacities of ~555 mAh/g at extremely high rates of 11 C. While the rate returned to 0.1 C, the capacity was recovered rapidly. Strikingly, the nanowires retained high-rate capabilities during the five cycle periods at high charge/discharge rates, as shown in Figure 4b. A specific capacity of ~1000 mAh/g was recovered when the charge/discharge rate was lowered again to 0.1 C when cycled up to 200 times and still remained capacity retention without obvious fading from 200 to 250th cycle. These results show that dodecanethiol-passivated Ge nanowires have high-power capability.

Galvanostatic Cycling at 55 °C and Rate Capability. To operate lithium-ion batteries at higher temperatures is a critical safety issue for many applications such as automobile and electronic devices. We have tested the cycle performance of dodecanethiol-passivated Ge nanowires at 55 °C at charge/discharge rates that ranged from 0.2 to 16 C in the voltage range 0.01–1.5 V, as shown in Figure 5. The initial discharge capacities of 1319, 1089, 983, 874, 709, 602, 456, and 362 mAh/g were obtained at 0.2, 0.4, 1, 2, 4, 7, 10, and 16 C, respectively. The received capacities were similar to the cycling performance obtained at room temperature. After coming back to 0.2 C after a cycle of 100 times, the capacity recovered to ~1000 mAh/g. The fairly stable capacity shows the thermal stability of dodecanethiol-passivated Ge nanowire as an anode material at high working temperatures.

TEM and XPS Studies of Dodecanethiol-Passivated Ge Nanowire Electrode after Electrochemical Cycling. To investigate the role of chemical passivation related to structure stability of Ge nanowire electrode after cycling tests, the electrode was extracted from cells for *ex situ* TEM study. Before cycling, the slurry composite comprises nanowires surrounded with PVDF and carbon black, as shown in Figure 6a. During the first lithiation charged to 0.01 V, crystalline Ge nanowires were mainly converted to amorphous Li_xGe wires, which was confirmed by SAED patterns showing the weak spots along with several diffuse rings, which probably originated from amorphous phases of Li_xGe alloy or Ge (Figure 6b).[14] The average diameter of nanowires increased to around 78 nm, which is larger than those before lithiation as expected as a result of volume expansion after lithium alloying reactions. Figure 6c shows TEM images of nanowires during first delithiation discharged to 1.5 V. The nanowires became mostly amorphous Ge.[14,38,64] Nanopores started to emerge inside the nanowire, similar to the structure observed in recent study of *in situ* TEM study for lithiation/delithiation behavior of Ge nanowires.[14] High diffusivity of Li in Ge may facilitate pore nucleate and grow during decrystallization. The nanosponges provide channels with better electrical conduction to allow Li atoms to

diffuse preferentially near the pore regions in subsequent cycles that could facilitate a high rate of lithium ion diffusion and stress relaxation due to shorter ion transport paths.[14] In contrast to disintegrated wires observed in unfunctionalized Ge nanowires, nanowires remained integrated in the form of a network composed of Ge nanowires and PVDF binder (Figure 6d). This result indicates that Ge nanowires must form a composite matrix with PVDF after Li insertion/extraction processes. After the second cycle, nanowire/PVDF composite structures could be more clearly observed (Figure 6 e,f). The structure stability of this composite was examined by long-term cycling tests (Figure 7).

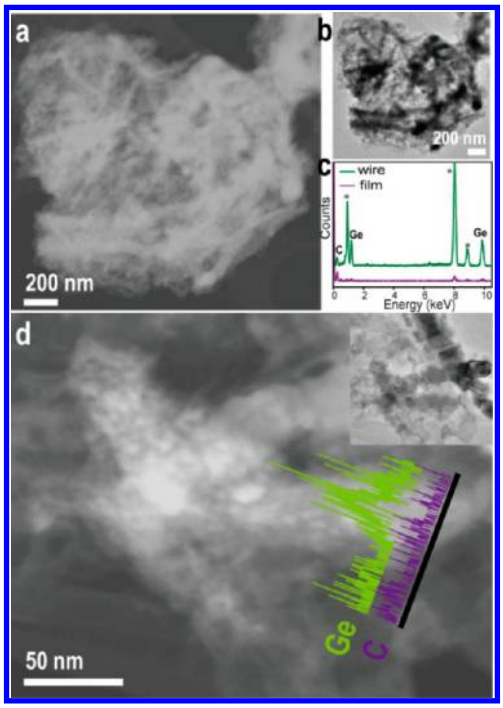

Figure 7. (a–c) Dodecanethiol-passivated Ge nanowires cycled for 100 cycles at a rate of 0.1 C in a lithium-ion cell: (a) HADDF image, (b) brightfield TEM image showing that the electrode composite remained a nanowire networks structure. (c) EDX analysis of bright and dark region of Ge nanowire network, respectively. Note that the asterisk (*) represents the Cu signal from the Cu TEM grid. (d) HADDF image and EDS line scan analysis of the Ge nanowire electrode after 50 cycles at a rate of 6.5 C. Inset: the corresponding TEM image.

Figure 7b show TEM images of the Ge nanowires showing a similar network structure at a rate of 0.1 C after 100 cycles. Under STEM mode (Figure 7a), the contrast between nanowires and PVDF were more obvious, clearly showing Ge nanowires encapsulated in the PVDF matrix (Figure 7a). Nanometer-scale energy dispersive X-ray spectra (EDS) of the networks confirmed that the high contrast portion is Ge and the lower contrast part is mainly composed of C (Figure 7c). The network structure remained at a high rate of 6.5 C after 50 cycles (Figure 7d). The continuous Ge nanowire network inside the PVDF provides both mechanical integrity and electrical interconnects through the whole composite. However, it could not be ruled out that some portion of nanowires might be degraded and embedded in the composite electrode. This structure could effectively accommodate mechanical stress by relaxing the external stress after repeated cycles of lithium insertion and extraction and avoid nanowire fracture. The benefit of its mechanical stability was reflected on the obtained superior electrochemical performance.

XPS spectra of C 1s peaks of dodecanethiol-passivated Ge nanowires taken before and after cycling at a rate of 0.1 C were performed (Figure 8). Before cycling tests, dodecanethiol–Ge nanowires had four C 1s peaks assigned to ~284.3, 286.0, 287.8, and 290.4 eV. The first peak at 284.3 eV corresponds to C–C/C=C and indicates carbon atoms unbound to fluorine which may be contributed from the carbon black and the functionalized layer of Ge nanowires. The second peak centered at 286.0 eV may include the contributions from C–O bonding and the carbon atoms adjacent to C–F bonds. The third peak centered at 287.8 eV may be attributed to an intermediate between a semi-ionic C–F bond, usually observed in fluorinated materials, C_xF, and a covalent C–F bond. The last C 1s peak centered at 290.4 eV may be the satellite plasmon peaks, which were normally observed in graphite samples and attributed to a small amount of covalent C–F bonds.[65–67] However, the third and fourth peaks were very weak, indicating a limited amount of carbon atoms on the Ge nanowire surface bound to the fluorine. After cycling tests, the peaks intensity related

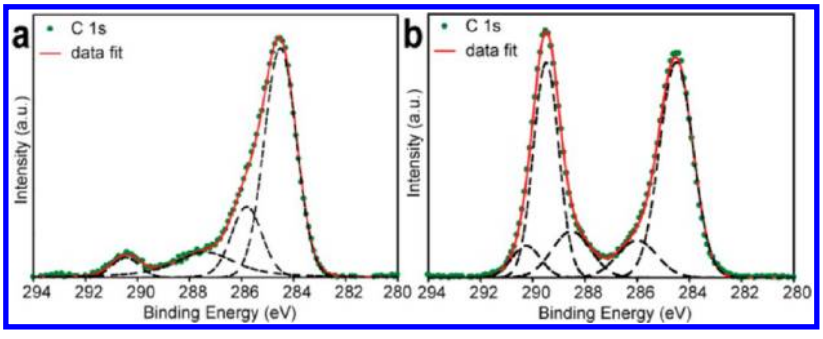

Figure 8. C 1s spectrum of Ge nanowire electrode composite (a) before and (b) after 30 cycles at a rate of 0.1 C.

to C−F bonding shifted to a higher binding energy along with a significant increase of peak intensity, indicating the enhanced covalency of the C−F bond. The enhanced bonding was usually observed in the fluorine−graphite intercalation compound and in fluorinated carbon black with increasing fluorine content. According to previous work,[68] it may be because dangling bonds of carbon atoms exist at the edges of amorphous carbon where neighboring carbon atoms are connected through weak C−H bonds. Importantly, the polymer was preferentially absorbed onto these imperfect sites, leading to C−F bonding formation.[69,70] Furthermore, PVDF might form a hydrogen bond between the F atoms and H atoms and was incorporated with inorganic minerals.[71] PVDF adsorbed onto the carbon site by C−F related bonds with dodecanethiol−functionalized Ge nanowires. The occurrence of a bonding intermediate between the semi-ionic and covalent C−F may lead to a stronger interaction between the nanowires so as to serve as an important source to maintain adhesion strength and structure stability of the functionalized Ge nanowires. It should be noted that the peaks of the unfunctionalized Ge nanowire after cycling tests have a smaller enhancement (Supporting Information, Figure S3), which might be due to weaker bonding between PVDF and oxided Ge nanowires. Better covalent bonding of dodecanethiol−Ge nanowires with PVDF is highly related to the structure integrity of Ge nanowires under the Li insertion/extraction reaction.

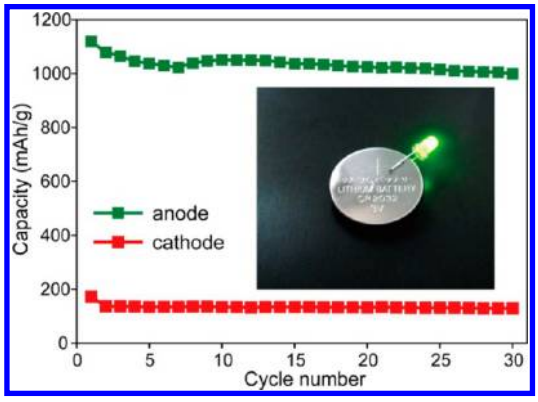

Figure 9. Capacity *versus* cycle number of a coin full cell between 2.0 and 3.8 V with dodecanethiol-passivated Ge nanowire as the anode and $LiFePO_4$ as the cathode. Photograph of Ge nanowire-based lithium-ion battery (CR2032) that lights a green LED up.

Full Cells Assembly and Testing. The incorporation of a Ge nanowire electrode into a lithium-ion full cell using $LiFePO_4$ particles as the cathode is demonstrated. Figure 9 shows the rate capability and cycling life of Ge nanowires and $LiFePO_4$ in a CR2032-type coin cell. The average discharge voltage of the full cell was ~3.4 V. The first and 30th discharge capacities of Ge nanowires were

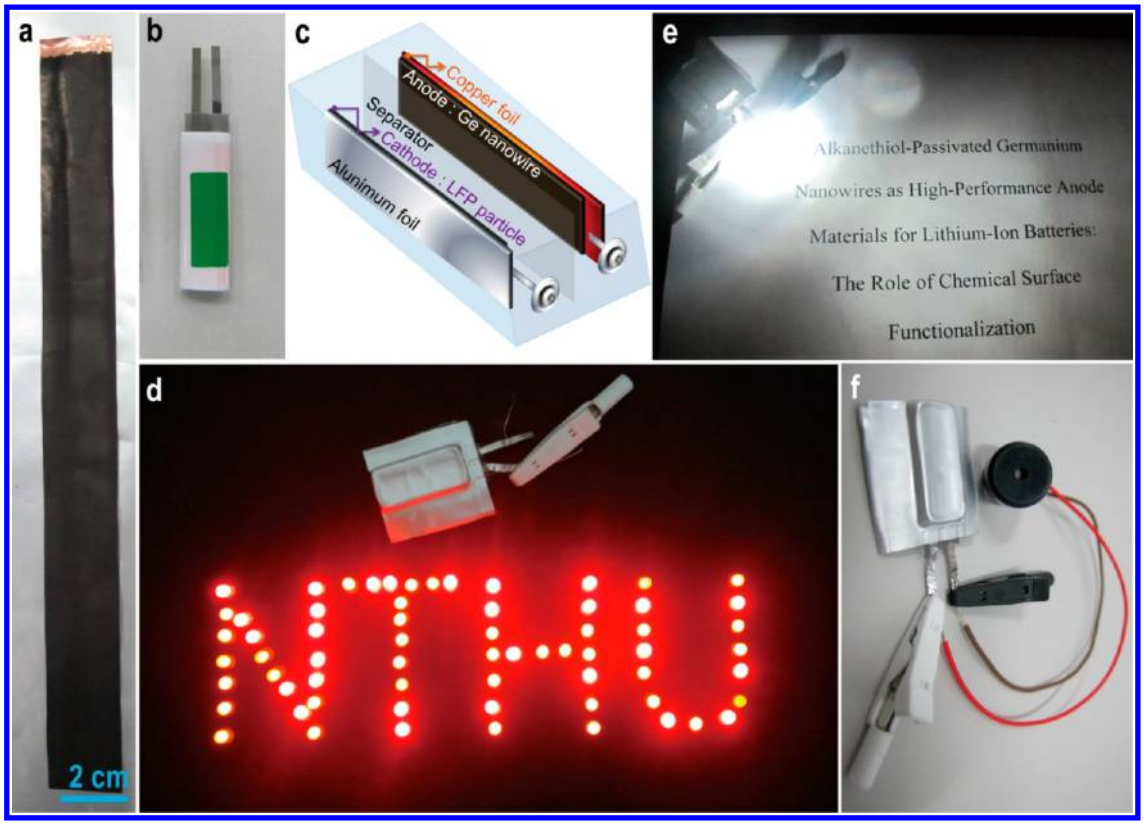

Figure 10. (a) A 2.2 × 22 cm Cu foil covered with an anode film of Ge nanowires. (b) Photograph of the assembled full cell before encapsulation in an aluminum bag. (c) Schematic of a lithium-ion battery with device structure using Ge nanowire anode and $LiFePO_4$ cathode on both sides. An aluminum pouch type lithium-ion battery (anode, Ge nanowires; cathode, $LiFePO_4$) used to (d) light up over 60 red LEDs, (e) a white LED bulb, and (f) an audio electronic device.

1119 and 1000 mAh/g, respectively. The received capacity was slightly lower than that obtained in the half cell since the capacity ratio of the anode/cathode was not optimized. However, the Ge nanowires still had good capacity retention of 90% over 30 cycles. The assembled full cell can draw a current intensity of ~1 mA which was able to light up a green light-emitting-diode (LED) (Figure 9 inset). A large size of Ge nanowire anode was directly incorporated into an aluminum pouch-type lithium battery. Figure 10a shows a 2.2 × 22 cm copper foil homogeneously covered with an anode film of Ge nanowires after drying at 150 °C in vacuum. The anode was then assembled using automatic cell lines in a dry room. Figure 10b shows the photograph of the assembled full cell before encapsulation in an aluminum bag. Figure 10c shows the components of the battery. The battery gave a larger current intensity (~30 mA) to light up over 60 red LEDs (Figure 10d) and a white LED bulb (Figure 10e), and to turn on an audio device (Figure 10f, Supporting Information, Video S1). After many instances of charge/discharge, this battery could be still reusable to light up the LEDs (Supporting Information, Figure S4).

CONCLUSION

Dodecanethiol-passivated Ge nanowires exhibit high reversible capacity, high-power capability, and stable cycle performance, thus demonstrating promising anode materials for high-energy density and high-power lithium-ion battery applications. The electrode has superior thermal stability while being operated at 55 °C. A lithium-ion full battery using dodecanethiol-passivated Ge nanowires as the anode and $LiFePO_4$ as the cathode was assembled for LEDs lighting and audio electronic devices, showing that Ge nanowires might be a viable alternative to graphite for higher capacity. The important role of surface functionalization for structure integrity associated with a Li insertion/extraction reaction was highlighted in this study. Under the process of multiple repeated high-rate charge/discharge cycles, dodecanethiol-passivated Ge nanowires formed a robust nanowire/PVDF network with good structure integrity, whereas unpassivated wires disintegrated to a Ge fragment species. Importantly for practical purposes, organic monolayer passivation offers an effective method to make low carbon containing Ge–C anode materials well-mixed with additive materials for high-quality electrode film fabrication. Moreover, the thiolation reactions can be applied to surface functionalization of a large quantity of material at low temperatures, thus being very compatible with commercial fabrication procedures.

METHODS

Materials. Diphenylgermane (DPG, 95%) was purchased from Gelest. Hydrogen tetrachloroaurate (III) trihydrate (99.99%), tetraoctylammoniumbromide (TOAB, 98%), sodium borohydride (98.0%), anhydrous benzene (99.8%), toluene (99.99%), 1-dodecanethiol (98.0%), ethanol (99.8%), hydrofluoric acid (48 wt %), and Ge powder (~100 mesh >99.99%) were purchased from Sigma-Aldrich. $LiPF_6$ (1.0 M in a 1:1 mixture of ethylene carbonate/dimethyl carbonate), Celgard membrane (as separator), Li metal foil (99.9%), Cu metal foil (0.01 mm), $LiFePO_4$ cathode electrode, PVDF, *N*-methyl-2-pyrrolidone (NMP, 99%) Super P carbon black, coin-type half-cells (CR2032), were purchased from SYNergy ScienTech Corp. LEDs were purchased from an electronic equipment and appliance store.

Ge Nanowire Synthesis. Ge nanowire reactions were carried out in a flow reaction in a 10 mL titanium grade-2 reactor.[72] The reactor was first placed into an argon-filled glovebox to make it free of oxygen, and then was brought out from the glovebox. The reactor cell was covered with heating tape and insulation with temperature maintained within ±1 °C controlled by a controller. The inlet and outlet of the 10 mL Ti reactor cell were attached to a high-pressure ($^1/_8$ in. i.d.) tubing *via* a LM-6 HIP (high pressure equipment Co.) reducer. The inlet tubing was collected to a six-way valve (Valco) attached with a 10 mL injection loop. A high pressure liquid chromatography (HPLC) pump (Lab Alliance, series 1500) connected to the six-way valve was used to deliver the reactant solution into the reactor and pressurize the reactor. The reactor pressure is monitored by a digital pressure gauge (Yan-Chang Technology). DPG was diluted in anhydrous benzene to a concentration of 500 mM in an argon-filled glovebox, followed by addition of dodecanethiol-capped Au nanoparticles with a Au/Ge molar ratio of 1:500. In nanowire synthesis, the reactor was heated to 420 °C and was pressurized to 800 psi. A 10 mL reactant solution loaded inside the injection loop was delivered to the reactor at a flow rate of 0.5 mL/min. The microcontrol metering valve was opened manually to keep the system pressure at 1000 psi. After the synthesis, the reactor cell was cooled by fresh air until it reached room temperature. The Ge nanowires were removed from the reactor for further uses.

Surface Passivation. Thiolation of Ge nanowires was carried out outside the supercritical fluid reactor. Nanowires were etched in 5% HF for 5 min, followed by rinse with DI water. The H-terminated Ge nanowires were transferred to a three-necked flask connected to a Schlenk line. After 20 mL of dodecanethiol added to immerse Ge nanowires, the flask was quickly purged of oxygen by argon. The reaction was held at 80 °C for 12 h at argon atmosphere. After thiolation, the dodecanethiol-passivated Ge nanowires were isolated by precipitation with addition of 10 mL of toluene and 10 mL of ethanol followed by centrifugation at 8000 rpm for 5 min. After a washing step, the functionalized Ge nanowires were redispersed in toluene.

Characterization. The chemical bonds of bulk metals were analyzed by a high resolution X-ray photoelectron spectrometer (XPS, PHI Quantera SXM/Auger: AES 650). Ge nanowires were characterized using scanning electron microscopy (SEM) and transmission electron microscopy (TEM). For HRSEM imaging, images were obtained using a HITACHI-S4700 field-emission SEM, operated at 5–15 kV accelerating voltage with working distances ranging between 10 to 20 mm. The TEM samples were prepared by either the drop-casting of nanowires from toluene dispersions onto 200-mesh lacey carbon-coated copper grids (Electron Microscope Sciences). Images were acquired using 200 accelerating voltage on a JEOL JEM-2100F, equipped with an Oxford INCA EDS spectrometer. For conducting *ex situ* TEM analysis of the samples after charge/discharge tests, the composite electrode was dissembled from the cell, and dispersed in acetone with ultrasonic treatment.

Lithium-Ion Battery Assembly and Electrochemical Characterization. The composite electrode was prepared by mixing active materials (75 wt %) with 10 wt % of Super P carbon black and 15 wt % of PVDF binder in *N*-methyl-2-pyrrolidinone (NMP) solvent to form a homogeneous slurry, which was then spread onto a copper foil. The weight of pure active material was measured using a microbalance with 0.1 μg resolution (Sartorius SE2). Typical anode mass loading is $\sim$1 mg/cm^2. The electrodes were dried at 40 °C in air and then 150 °C under Ar gas prior to cell assembling in order to remove any residual water. The coin-type half-cells (CR2032), prepared in an argon-filled glovebox, contained a Ge nanowires electrode, Li metal foil, and microporous polyethylene separator soaked in electrolyte. The electrolyte solution was 1 M $LiPF_6$ in ethylene carbonate/dimethyl carbonate (EC/DMC) (1:1 vol %). The electrochemical performance of the Ge nanowires was evaluated using Biologic VMP3 instruments. For full cell assembly, the $LiFePO_4$ electrode with a loading mass of $\sim$8 mg/cm^2 was used as a cathode, whereas the anode mass loading remained at 1 mg/cm^2. The electrochemical properties of the full cells were examined at 0.1 C rate in voltage windows between 2.0 and 3.8 V with the same experimental system. The electrode capacity was calculated according to the weight of the active materials.

Conflict of Interest: The authors declare no competing financial interest.

Supporting Information Available: TEM images and XPS of unpassivated Ge nanowires; TEM images of unpassivated Ge nanowires after cycling tests; XPS of unpassivated Ge nanowire electrode after cycling tests; more images of LEDs lighted by the aluminum pouch-type lithium battery; movie (MPG) showing the use of a battery to operate an audio device. This material is available free of charge *via* the Internet at http://pubs.acs.org.

Acknowledgment. The authors acknowledge the financial support by the National Science Council of Taiwan (NSC 99-2221-E-007-096, NSC 100-3113-E-007-008, NSC 100-2628-E-007-029-MY2), the Minitry of Economic Affairs, Taiwan (101-EC-17-A-09-S1-198), National Tsing Hua University (100N2060E1, 100N2041E1), the HRTEM (JEOL JEM-2100F) assistance from Tamkang University College of Science, and the assistance from Center for Energy and Environmental Research, National Tsing-Hua University.

REFERENCES AND NOTES

1. Cheng, F. Y.; Liang, J.; Tao, Z. L.; Chen, J. Functional Materials for Rechargeable Batteries. *Adv. Mater.* **2011**, *23*, 1695–1715.
2. Bruce, P. G.; Scrosati, B.; Tarascon, J. M. Nanomaterials for Rechargeable Lithium Batteries. *Angew. Chem. Int. Ed.* **2008**, *47*, 2930–2946.
3. Scrosati, B.; Hassoun, J.; Sun, Y. K. Lithium-Ion Batteries: A Look into the Future. *Energy Environ. Sci.* **2011**, *4*, 3287–3295.
4. Yoshio, M.; Tsumura, T.; Dimov, N. Electrochemical Behaviors of Silicon Based Anode Material. *J. Power Sources* **2005**, *146*, 10–14.
5. Kasavajjula, U.; Wang, C. S.; Appleby, A. Nano- and Bulk-Silicon-Based Insertion Anodes for Lithium-Ion Secondary Cells. *J. Power Sources* **2007**, *163*, 1003–1039.
6. Wang, X. L.; Feygenson, M.; Chen, H. Y.; Lin, C. H.; Ku, W.; Bai, J. M.; Aronson, M. C.; Tyson, T. A.; Han, W. Q. Nanospheres of a New Intermetallic $FeSn_5$ Phase: Synthesis, Magnetic Properties and Anode Performance in Li-Ion Batteries. *J. Am. Chem. Soc.* **2011**, *133*, 11213–11219.
7. Baggetto, L.; Hensen, E. J. M.; Notten, P. H. L. *In Situ* X-ray Absorption Spectroscopy of Germanium Evaporated Thin Film Electrodes. *Electrochim. Acta* **2010**, *55*, 7074–7079.
8. Wang, X. L.; Han, W. Q.; Chen, H. Y.; Bai, J. M.; Tyson, T. A.; Yu, X. Q.; Wang, X. J.; Yang, X. Q. Amorphous Hierarchical Porous GeOx as High-Capacity Anodes for Li Ion Batteries with Very Long Cycling Life. *J. Am. Chem. Soc.* **2011**, *133*, 20692–20695.
9. Guo, W.; Xue, X.; Wang, S.; Lin, C; Wang, Z. L. An Integrated Power Pack of Dye-Sensitized Solar Cell and Li Battery Based on Double-Sided TiO_2 Nanotube Arrays. *Nano Lett.* **2012**, *12*, 2520–2523.
10. Simon, P.; Gogotsi, Y. Materials for Electrochemical Capacitors. *Nat. Mater.* **2008**, *7*, 845–854.
11. Park, C. M.; Kim, J. H.; Kim, H.; Sohn, H. J. Li-Alloy Based Anode Materials for Li Secondary Batteries. *Chem. Soc. Rev.* **2010**, *39*, 3115–3141.
12. Zhang, W. J. A Review of the Electrochemical Performance of Alloy Anodes for Lithium-Ion Batteries. *J. Power Sources* **2011**, *196*, 13–24.
13. Cheng, F. Y.; Liang, J.; Tao, Z. L.; Chen, J. Functional Materials for Rechargeable Batteries. *Adv. Mater.* **2011**, *23*, 1695–1715.
14. Liu, X. H.; Huang, S.; Picraux, S. T.; Li, J.; Zhu, T.; Huang, J. Y. Reversible Nanopore Formation in Ge Nanowires during Lithiation–Delithiation Cycling: An *In Situ* Transmission Electron Microscopy Study. *Nano Lett.* **2011**, *11*, 3991–3997.
15. Prabakar, S.; Shiohara, A.; Hanada, S.; Fujioka, K.; Yamamoto, K.; Tilley, R. D. Size Controlled Synthesis of Germanium Nanocrystals by Hydride Reducing Agents and Their Biological Applications. *Chem. Mater.* **2010**, *22*, 482–486.
16. Warner, J. H.; Tilley, R. D. Synthesis of Water-Soluble Photoluminescent Germanium Nanocrystals. *Nanotechnology* **2006**, *17*, 3745–3749.
17. Codoluto, S. C.; Baumgardner, W. J.; Hanrath, T. Fundamental Aspects of Nucleation and Growth in the Solution-Phase Synthesis of Germanium Nanocrystals. *Crystengcomm* **2010**, *12*, 2903–2909.
18. Lu, X. M.; Korgel, B. A.; Johnston, K. P. High Yield of Germanium Nanocrystals Synthesized from Germanium Diiodide in Solution. *Chem. Mater.* **2005**, *17*, 6479–6485.
19. Lu, X. M.; Ziegler, K. J.; Ghezelbash, A.; Johnston, K. P.; Korgel, B. A. Synthesis of Germanium Nanocrystals in High Temperature Supercritical Fluid Solvents. *Nano Lett.* **2004**, *4*, 969–974.
20. Henderson, E. J.; Hessel, C. M.; Veinot, J. G. C. Synthesis and Photoluminescent Properties of Size-Controlled Germanium Nanocrystals from Phenyl Trichlorogermane-Derived Polymers. *J. Am. Chem. Soc.* **2008**, *130*, 3624–3632.
21. Park, M. H.; Kim, K.; Kim, J.; Cho, J. Flexible Dimensional Control of High-Capacity Li-Ion-Battery Anodes: From 0D Hollow to 3D Porous Germanium Nanoparticle Assemblies. *Adv. Mater.* **2010**, *22*, 415–418.
22. Mullane, E.; Geaney, H.; Ryan, K. M. Size Controlled Growth of Germanium Nanorods and Nanowires by Solution Pyrolysis Directly on a Substrate. *Chem. Commun.* **2012**, *48*, 5446–5448.
23. Geaney, H.; Dickinson, C.; Barrett, C. A.; Ryan, K. M. High Density Germanium Nanowire Growth Directly from Copper Foil by Self-Induced Solid Seeding. *Chem. Mater.* **2011**, *23*, 4838–4843.
24. Barrett, C. A.; Geaney, H.; Gunning, R. D.; Laffir, F. R.; Ryan, K. M. Perpendicular Growth of Catalyst-free Germanium Nanowire Arrays. *Chem. Commun.* **2011**, *47*, 3843–3845.
25. Barrett, C. A.; Gunning, R. D.; Hantschel, T.; Arstila, K.; O'Sullivan, C.; Geaney, H.; Ryan, K. M. Metal Surface Nucleated Supercritical Fluid–Solid–Solid Growth of Si and Ge/SiO_x Core–Shell Nanowires. *J. Mater. Chem.* **2010**, *20*, 135–144.
26. Wu, Y. Y.; Fan, R.; Yang, P. D. Block-by-Block Growth of Single-Crystalline Si/SiGe Superlattice Nanowires. *Nano Lett.* **2002**, *2*, 83–86.
27. Hanrath, T.; Korgel, B. A. Nucleation and Growth of Germanium Nanowires Seeded by Organic Monolayer-Coated Gold Nanocrystals. *J. Am. Chem. Soc.* **2002**, *124*, 1424–1429.
28. Hobbs, R. G.; Barth, S.; Petkov, N.; Zirngast, M.; Marschner, C.; Morris, M. A.; Holmes, J. D. Seedless Growth of Sub-10 nm Germanium Nanowires. *J. Am. Chem. Soc.* **2010**, *132*, 13742–13749.
29. Lu, X. M.; Fanfair, D. D.; Johnston, K. P.; Korgel, B. A. High Yield Solution-Liquid–Solid Synthesis of Germanium Nanowires. *J. Am. Chem. Soc.* **2005**, *127*, 15718–15719.

30. Wang, D. W.; Dai, H. J. Low-Temperature Synthesis of Singl-Crystal Germanium Nanowires by Chemical Vapor Deposition. *Angew. Chem. Int. Ed.* **2002**, *41*, 4783.
31. Gerung, H.; Boyle, T. J.; Tribby, L. J.; Bunge, S. D.; Brinker, C. J.; Han, S. M. Solution Synthesis of Germanium Nanowires Using a Ge_2^+ Alkoxide Precursor. *J. Am. Chem. Soc.* **2006**, *128*, 5244–5250.
32. Wu, Y. Y.; Yang, P. D. Germanium Nanowire Growth *via* Simple Vapor Transport. *Chem. Mater.* **2000**, *12*, 605–607.
33. Tuan, H. Y.; Lee, D. C.; Hanrath, T.; Korgel, B. A. Germanium Nanowire Synthesis: An Example of Solid-Phase Seeded Growth with Nickel Nanocrystals. *Chem. Mater.* **2005**, *17*, 5705–5711.
34. Mathur, S.; Shen, H.; Donia, N.; Rugamer, T.; Sivakov, V.; Werner, U. One-Step Chemical Vapor Growth of Ge/SiC_xN_y Nanocables. *J. Am. Chem. Soc.* **2007**, *129*, 9746–9752.
35. Park, M. H.; Cho, Y.; Kim, K.; Kim, J.; Liu, M. L.; Cho, J. Germanium Nanotubes Prepared by Using the Kirkendall Effect as Anodes for High-Rate Lithium Batteries. *Angew. Chem. Int. Ed.* **2011**, *50*, 9647–9650.
36. Liu, N.; Hu, L.; McDowell, M. T.; Jackson, A.; Cui, Y. Prelithiated Silicon Nanowires as an Anode for Lithium Ion Batteries. *ACS Nano* **2011**, *5*, 6487–6493.
37. Chan, C. K.; Peng, H. L.; Liu, G.; McIlwrath, K.; Zhang, X. F.; Huggins, R. A.; Cui, Y. High-Performance Lithium Battery Anodes Using Silicon Nanowires. *Nat. Nanotechnol.* **2008**, *3*, 31–35.
38. Chan, C. K.; Zhang, X. F.; Cui, Y. High Capacity Li Ion Battery Anodes Using Ge Nanowires. *Nano Lett.* **2008**, *8*, 307–309.
39. Chan, C. K.; Patel, R. N.; O'Connell, M. J.; Korgel, B. A.; Cui, Y. Solution-Grown Silicon Nanowires for Lithium-Ion Battery Anodes. *ACS Nano* **2010**, *4*, 1443–1450.
40. Seo, M. H.; Park, M.; Lee, K. T.; Kim, K.; Kim, J.; Cho, J. High Performance Ge Nanowire Anode Sheathed with Carbon for Lithium Rechargeable Batteries. *Energy Environ. Sci.* **2011**, *4*, 425–428.
41. Wang, X. L.; Han, W. Q. Graphene Enhances Li Storage Capacity of Porous Single-Crystalline Silicon Nanowires. *ACS Appl. Mater. Inter.* **2010**, *2*, 3709–3713.
42. Chockla, A. M.; Panthani, M. G.; Holmberg, V. C.; Hessel, C. M.; Reid, D. K.; Bogart, T. D.; Harris, J. T.; Mullins, C. B.; Korgel, B. A. Electrochemical Lithiation of Graphene-Supported Silicon and Germanium for Rechargeable Batteries. *J. Phys. Chem. C* **2012**, *116*, 11917–11923.
43. Tan, L.; Lu, Z.; Tan, H. T.; Zhu, J.; Rui, X.; Yan, Q.; Hng, H. H. Germanium Nanowires-Based Carbon Composite as Anodes for Lithium-Ion Batteries. *J. Power Sources* **2012**, *206*, 253–258.
44. Yao, Y.; Huo, K.; Hu, L.; Liu, N; Cha, J. J.; McDowell, M. T.; Cui, Y. Highly Conductive, Mechanically Robust, and Electrochemically Inactive TiC/C Nanofiber Scaffold for High-Performance Silicon Anode Batteries. *ACS Nano* **2011**, *5*, 8346–8351.
45. Lee, H.; Kim, H.; Doo, S. G.; Cho, J. Synthesis and Optimization of Nanoparticle Ge Confined in a Carbon Matrix for Lithium Battery Anode Material. *J. Electrochem. Soc.* **2007**, *154*, A343–A346.
46. Kim, H.; Cho, J. Superior Lithium Electroactive Mesoporous Si@Carbon Core–Shell Nanowires for Lithium Battery Anode Material. *Nano Lett.* **2008**, *8*, 3688–3691.
47. Chockla, A. M.; Harris, J. T.; Akhavan, V. A.; Bogart, T. D.; Holmberg, V. C.; Steinhagen, C.; Mullins, C. B.; Stevenson, K. J.; Korgel, B. A. Silicon Nanowire Fabric as a Lithium Ion Battery Electrode Material. *J. Am. Chem. Soc.* **2011**, *133*, 20914–20921.
48. DiLeo, R. A.; Frisco, S.; Ganter, M. J.; Rogers, R. E.; Raffaelle, R. P.; Landi, B. J. Hybrid Germanium Nanoparticle-Single-Wall Carbon Nanotube Free-Standing Anodes for Lithium Ion Batteries. *J. Phys. Chem. C* **2011**, *115*, 22609–22614.
49. Collins, G.; Holmes, J. D. Chemical Functionalisation of Silicon and Germanium Nanowires. *J. Mater. Chem.* **2011**, *21*, 11052–11069.
50. Hanrath, T.; Korgel, B. A. Chemical Surface Passivation of Ge Nanowires. *J. Am. Chem. Soc.* **2004**, *126*, 15466–15472.
51. Holmberg, V. C.; Korgel, B. A. Corrosion Resistance of Thiol- and Alkene-Passivated Germanium Nanowires. *Chem. Mater.* **2010**, *22*, 3698–3703.
52. Wang, D. W.; Chang, Y. L.; Liu, Z.; Dai, H. J. Oxidation Resistant Germanium Nanowires: Bulk Synthesis, Long Chain Alkanethiol Functionalization, and Langmuir-Blodgett Assembly. *J. Am. Chem. Soc.* **2005**, *127*, 11871–11875.
53. Smith, D. A.; Holmberg, V. C.; Rasch, M. R.; Korgel, B. A. Optical Properties of Solvent-Dispersed and Polymer-Embedded Germanium Nanowires. *J. Phys. Chem. C* **2010**, *114*, 20983–20989.
54. Shiohara, A.; Hanada, S.; Prabakar, S.; Fujioka, K.; Lim, T. H.; Yamamoto, K.; Northcote, P. T.; Tilley, R. D. Chemical Reactions on Surface Molecules Attached to Silicon Quantum Dots. *J. Am. Chem. Soc.* **2010**, *132*, 248–253.
55. Buriak, J. M. Organometallic Chemistry on Silicon and Germanium Surfaces. *Chem. Rev.* **2002**, *102*, 1271–1308.
56. Hanrath, T.; Korgel, B. A. Influence of Surface States on Electron Transport through Intrinsic Ge Nanowires. *J. Phys. Chem. B* **2005**, *109*, 5518–5524.
57. Collins, G.; Fleming, P.; O'Dwyer, C.; Morris, M. A.; Holmes, J. D. Organic Functionalization of Germanium Nanowires using Arenediazonium Salts. *Chem. Mater.* **2011**, *23*, 1883–1891.
58. Collins, G.; Fleming, P.; Barth, S.; O'Dwyer, C.; Boland, J. J.; Morris, M. A.; Holmes, J. D. Alkane and Alkanethiol Passivation of Halogenated Ge Nanowires. *Chem. Mater.* **2010**, *22*, 6370–6377.
59. Holmberg, V. C.; Rasch, M. R.; Korgel, B. A. PEGylation of Carboxylic Acid-Functionalized Germanium Nanowires. *Langmuir* **2010**, *26*, 14241–14246.
60. Wang, D. W.; Chang, Y. L.; Wang, Q.; Cao, J.; Farmer, D. B.; Gordon, R. G.; Dai, H. J. Surface Chemistry and Electrical Properties of Germanium Nanowires. *J. Am. Chem. Soc.* **2004**, *126*, 11602–11611.
61. Loscutoff, P. W.; Bent, S. F. Reactivity of the Germanium Surface: Chemical Passivation and Functionalization. *Annu. Rev. Phys. Chem.* **2006**, *57*, 467–495.
62. Tuan, H. Y.; Korgel, B. A. Importance of Solvent-Mediated Phenylsilane Decompositon Kinetics for High-Yield Solution-Phase Silicon Nanowire Synthesis. *Chem. Mater.* **2008**, *20*, 1239–1241.
63. Heitsch, A. T.; Fanfair, D. D.; Tuan, H. Y.; Korgel, B. A. Solution–Liquid–Solid (SLS) Growth of Silicon Nanowires. *J. Am. Chem. Soc.* **2008**, *130*, 5436–5437.
64. Ko, Y. D.; Kang, J. G.; Lee, G. H.; Park, J. G.; Park, K. S.; Jin, Y. H.; Kim, D. W. Sn-Induced Low-Temperature Growth of Ge Nanowire Electrodes with a Large Lithium Storage Capacity. *Nanoscale* **2011**, *3*, 3371–3375.
65. Nakahara, M.; Ozawa, K.; Sanada, Y. Change in the Chemical Structures of Carbon-Black and Active-Carbon Caused by CF_4 Plasma Irradiation. *J. Mater. Sci.* **1994**, *29*, 1646–1651.
66. Koh, M.; Yumoto, H.; Higashi, H.; Nakajima, T. Fluorine Intercalation in Carbon Alloy C_xN. *J. Fluorine. Chem.* **1999**, *97*, 239–246.
67. Nakajima, T.; Koh, M.; Singh, R. N.; Shimada, M. Electrochemical Behavior of Surface-Fluorinated Graphite. *Electrochim. Acta* **1999**, *44*, 2879–2888.
68. Wang, Z. X.; Huang, X. J.; Xue, R. J.; Chen, L. Q. A New Possible Mechanism of Lithium Insertion and Extraction in Low-Temperature Pyrolytic Carbon Electrode. *Carbon* **1999**, *37*, 685–692.
69. Yoo, M.; Frank, C. W.; Mori, S. Interaction of Poly(vinylidene fluoride) with Graphite Particles. 1. Surface Morphology of a Composite Film and its Relation to Processing Parameters. *Chem. Mater.* **2003**, *15*, 850–861.
70. Yoo, M.; Frank, C. W.; Mori, S.; Yamaguchi, S. Effect of Poly(vinylidene fluoride) Binder Crystallinity and Graphite Structure on the Mechanical Strength of the Composite Anode in a Lithium Ion Battery. *Polymer* **2003**, *44*, 4204.
71. Yano, S.; Iwata, K.; Kurita, K. Physical Properties and Structure of Organic–Inorganic Hybrid Materials Produced by Sol–Gel Process. *Mat. Sci. Eng. C.-Bio. S.* **1998**, *6*, 75–90.

72. Yuan, F. W.; Yang, H. J.; Tuan, H. Y. Seeded Silicon Nanowire Growth Catalyzed by Commercially Available Bulk Metals: Broad Selection of Metal Catalysts, Superior Field Emission Performance, and Versatile Nanowire/Metal Architectures. *J. Mater. Chem.* **2011**, *21*, 13793–13800.